arXiv:1606.02160v1 [physics.flu-dyn] 7 Jun 2016

Optimal fluxes and Reynolds stresses

By Javier Jiménez

School of Aeronautics, Universidad Politécnica de Madrid, 28040 Madrid, Spain

(Received 8 June 2016)

It is remarked that fluxes in conservation laws, such as the Reynolds stresses in the momentum equation of turbulent shear flows, or the spectral energy flux in isotropic turbulence, are only defined up to an arbitrary solenoidal field. While this is not usually significant for long-time averages, it becomes important when fluxes are modelled locally in large-eddy simulations, or in the analysis of intermittency and cascades. As an example, a numerical procedure is introduced to compute fluxes in scalar conservation equations in such a way that their total integrated magnitude is minimised. The result is an irrotational vector field that derives from a potential, thus minimising sterile flux 'circuits'. The algorithm is generalised to tensor fluxes and applied to the transfer of momentum in a turbulent channel. The resulting instantaneous Reynolds stresses are compared with their traditional expressions, and found to be substantially different.

1. Introduction

Conservation laws are staples of continuum mechanics. They take the form of the rate of change of a conserved quantity ρ, such as mass, energy or momentum density, balanced by the divergence of a vector flux $\boldsymbol{\phi} = \{\phi_j\}$,

$$\partial_t \rho + \partial_j \phi_j = \widetilde{S}, \tag{1.1}$$

where ∂_j is the partial derivative along the j-th coordinate, repeated indices imply summation over all coordinate directions, and $\widetilde{S}$ represents any sources or sinks. While the physical significance of the conserved quantity is usually obvious, that of the flux is less clear, because only its divergence enters the equation. In spite of this, the fluxes themselves are often given physical significance, such as when Reynolds stresses are taken to represent the flux of momentum and are explicitly modelled in large-eddy simulations, or when a constant energy transfer rate is used as the basic parameter in the spectral theory of the turbulence cascade (Kolmogorov 1941). The cascade theories that form the backbone of modern turbulence research are not theories about conserved quantities, but about their fluxes.

A consequence of these considerations is that fluxes cannot be uniquely defined. Consider the generalisation of e̊q:conserv,

$$\partial_j \phi_j = \widetilde{S} - \partial_t \rho \equiv S, \tag{1.2}$$

where S has been modified to include the instantaneous temporal rate of change of the densities, and $\boldsymbol{\phi}$ is a vector flux in an n-dimensional space. In the first place, there is often some ambiguity in which part of S is incorporated into the flux, such as, for example, when a constant pressure gradient g is interpreted as a secular term gx_j within the corresponding spatial flux. But, even if that decomposition is decided on physical or other grounds, the definition of the fluxes remains ambiguous. The relation e̊q:divn is

singular when interpreted as an equation for the vector flux $\boldsymbol{\phi}$, given the source S. For example, any solenoidal vector field can be added to $\boldsymbol{\phi}$ without changing åeq:divn, and a three-dimensional vector flux is only defined up to the addition of a rotor.

This ambiguity is a particular case of the gauge invariance familiar from electromagnetic and other field theories (Barut 1980), and it should be clear that it in no way invalidates the original field equations. As in the case of other classical field theories, it only becomes important when trying to give physical significance to quantities that only appear in the equations as a gradient or as a divergence. In those cases, gauge transformations provides an extra degree of freedom in our choice of expression for the fluxes that can be used to simplify further manipulations for specific purposes. However, the extra gauge freedom implies that only gauge invariant quantities should be considered to be physically relevant. For example, we will see below that the energy–momentum tensor of classical fluid mechanics can be gauge-transformed. The same is true of its modelling counterpart, the Reynolds or sub-grid stresses. This suggests that neither of them should be a primary object of analysis, and that both should only be used as one among many possible representations of the same physical object. Which representation to use in each particular case should be decided on utilitarian, rather than on absolute grounds.

It should be noted that any two representations of the fluxes are linked by their divergence. As a consequence, if a particular expression R_j is known for the fluxes, there is no need to compute the right-hand side of åeq:divn. All other fluxes satisfy

$$\partial_j \phi_j = \partial_j R_j = S. \tag{1.3}$$

This paper describes a gauge designed to minimise a particular norm of $\boldsymbol{\phi}$. Although these 'optimal' fluxes have some useful properties, the emphasis is not so much on them as on their comparison with fluxes defined in more classical ways. The main goal is to determine whether different gauges result in very different flux properties, and how this can be used to differentiate properties that are intrinsic to the physics from those linked to a particular gauge. The paper is organised as follows. Optimal fluxes for scalar conservation laws are introduced in §2, and generalised to tensor fluxes of vector equations in §2.1. The methodology thus developed is applied to the stress tensor of the momentum conservation equation for a turbulent channel in §3, and the results are compared to the classical Reynolds-stress tensor in §4. Conclusions and possible directions for future research are offered in §5.

2. Optimal fluxes

As an example of the previous considerations, we will develop expressions for a set of 'optimal' fluxes that minimise the integrated flux magnitude over a domain of interest Ω. It should be emphasized that this definition is not unique, and that it is only optimum in the sense of minimising a particular norm. In general, choosing another norm or even another domain results in a different expression, but we shall see that such fluxes have sometimes a physically reasonable interpretation and that, as mentioned above, comparing two alternative definitions may be useful to determine which properties of the classically defined expressions are intrinsic to the physics, and which ones are accidents of a particular choice of gauge. Define a cost function,

$$J = \int_\Omega \left[\phi_j \phi_j/2 + \lambda(\partial_j \phi_j - S)\right] \mathrm{d}\Omega, \tag{2.1}$$

where åeq:divn has been added as a constraint with the scalar Lagrange multiplier λ. Taking the first variation, $\phi_j \to \phi_j + \delta\phi_j$, and integrating by parts, we obtain

$$\delta J = \int_\Omega (\phi_j - \partial_j \lambda)\, \delta\phi_j \,\mathrm{d}\Omega + \int_{\partial\Omega} \lambda\, \delta\phi_n \,\mathrm{d}(\partial\Omega) = 0, \tag{2.2}$$

where $\partial\Omega$ is the boundary of Ω, and the 'n' subscript denotes components normal to $\partial\Omega$. Requiring åeq:var1 to be satisfied for arbitrary $\delta\boldsymbol{\phi}$ yields the Euler variational equations (Gelfand & Fomin 1963),

$$\phi_j = \partial_j \lambda, \tag{2.3}$$

with natural boundary conditions,

$$\lambda = 0 \quad \text{at} \quad \partial\Omega. \tag{2.4}$$

The latter may require modification in especial cases. For example, if the fluxes are assumed to be spatially periodic along some direction, λ can also be assumed to be periodic. Equation åeq:varphi expresses the intuitive condition that the optimum flux should be an (irrotational) gradient, 'as free as possible' from circuits. When combined with the dynamical relation åeq:divn, the potential λ satisfies the Poisson equation,

$$\nabla^2 \lambda = S, \tag{2.5}$$

with homogeneous Dirichlet boundary conditions. Note that this does not imply that the fluxes vanish at the boundary, but applying Gauss theorem to åeq:divnR shows that

$$\int_{\partial\Omega} \phi_n \,\mathrm{d}(\partial\Omega) = \int_{\partial\Omega} R_n \,\mathrm{d}(\partial\Omega). \tag{2.6}$$

The total flux across the boundary is independent of the representation.

2.1. *Tensor fluxes*

Equation åeq:divn can be generalised to a vector right-hand side $\boldsymbol{S} = \{S_i\}$, such as momentum, and to a tensor flux $\boldsymbol{\Phi} = \{\phi_{ij}\}$,

$$\partial_j \phi_{ij} = S_i. \tag{2.7}$$

The potential is then a vector $\boldsymbol{\lambda} = \{\lambda_i\}$, and the problem can be defined as minimising the integrated Euclidean norm of the tensor. However, it is often the case that $\boldsymbol{\Phi}$ is not fully arbitrary, and the minimisation has to consider additional constraints. For example, the momentum flux tensor should be symmetric, in which case the cost function is

$$J = \int_\Omega [\phi_{ij}\phi_{ij}/2 + \lambda_i(\partial_j \phi_{ij} - S_i) + \varepsilon_{mij}\mu_m \phi_{ij}] \,\mathrm{d}\Omega, \tag{2.8}$$

where ε_{mij} is the completely antisymmetric Levi–Civita symbol, and the μ_m are extra Lagrange multipliers to ensure the symmetry of ϕ_{ij}. The Euler equations are then

$$\phi_{ij} = \partial_j \lambda_i - \varepsilon_{mij}\mu_m, \tag{2.9}$$

with natural boundary conditions as in åeq:varbc. The requirement that $\phi_{ij} = \phi_{ji}$ implies

$$\varepsilon_{mij}\mu_m = (\partial_j \lambda_i - \partial_i \lambda_j)/2, \tag{2.10}$$

and åeq:varphij becomes

$$\phi_{ij} = (\partial_j \lambda_i + \partial_i \lambda_j)/2. \tag{2.11}$$

Substituting in åeq:divn2 results in

$$\nabla(\nabla\cdot\boldsymbol{\lambda}) + \nabla^2\boldsymbol{\lambda} = 2\nabla(\nabla\cdot\boldsymbol{\lambda}) - \nabla\times\nabla\times\boldsymbol{\lambda} = 2\boldsymbol{S}. \tag{2.12}$$

This vector equation proves that $\boldsymbol{\lambda}$ is a cartesian vector, and that $\boldsymbol{\Phi}$ is a cartesian tensor. A useful equation for the trace of $\boldsymbol{\Phi}$, $\Pi = \phi_{ii} = \nabla \cdot \boldsymbol{\lambda}$, is obtained taking the divergence of åeq:poisvec,

$$\nabla^2 \Pi = \nabla \cdot \boldsymbol{S}. \tag{2.13}$$

If desired, Π can be separated from $\boldsymbol{\Phi}$ as a pressure-like isotropic term, and åeq:poisdiv becomes a variant of the usual pressure equation. In fact, the procedure leading to åeq:varphi–åeq:pois is akin to the classical derivation of the pressure equation in incompressible flows, and $\boldsymbol{\Phi}$ can be loosely interpreted as a generalised 'tensor pressure' that completes the right-hand side of åeq:divn2 in the same sense that the standard scalar pressure projects the momentum equation onto the incompressible subspace. On the other hand, the interpretation of the optimal tensor flux is not as straightforward as for a vector, since there is nothing like a rotor to justify the interpretation of 'minimum circularity'. The condition of minimum magnitude remains.

3. Momentum transfer in a turbulent channel

We illustrate the above procedure by computing the optimal momentum fluxes in a pressure-driven incompressible turbulent channel between infinite parallel plates separated by $2h$. As mentioned above, our main purpose is to determine how different are the optimal momentum fluxes from the classical Reynolds stresses, and thereby which properties of the latter should be considered physical and which ones accidental. We denote by x_i, with $i = 1$ to 3, the streamwise, wall-normal and spanwise coordinates, respectively, with $x_2 = 0$ at the lower wall. Momentum is injected across the channel cross-section by the streamwise gradient g_1 of the kinematic pressure, uniform in space but not necessarily in time. The spanwise pressure gradient vanishes at all times. Momentum is removed at the walls by viscous friction, and has to be transferred along x_2 from the body of the flow to the wall. The resulting flux is conserved except for the constant pressure forcing, and its conservation is responsible for the possibility of using the friction velocity u_τ as a uniform velocity scale at all wall distances (Townsend 1976). Quantities normalised with u_τ and with the kinematic viscosity ν are denoted by a '+' superscript.

The structures responsible for this transfer have been studied often. A recent summary can be found in Lozano-Durán *et al.* (2012), where it is shown that three-dimensional 'quadrant' structures (Wallace *et al.* 1972; Lu & Willmarth 1973) exist at all scales, and that the most intense ones form a self-similar hierarchy of sweeps and ejections with sizes proportional to their distance to the wall. Because of this size stratification, it can be argued that the momentum transfer constitutes an inertial turbulent cascade taking place mostly in space (Jiménez 2012, 2013*b*), although different from the energy cascade in Kolmogorov (1941). However, the non-uniqueness of the fluxes raises the question of the generality of these structures and of their properties.

The momentum equation can be written as

$$\partial_j \phi_{ij} = -\partial_t u_i - g_i, \tag{3.1}$$

which is satisfied by

$$\phi_{ij} = R_{ij} \equiv u_i u_j + p\delta_{ij} - 2\nu\sigma_{ij}, \tag{3.2}$$

where $\sigma_{ij} = (\partial_i u_j + \partial_j u_i)/2$ is the rate-of-strain tensor, and δ_{ij} is Kronecker's delta. The left-hand side of åeq:NS1 has been written in the form of a divergence, but we will see below by direct calculation that the tensor flux R_{ij} is not optimal. We are not aware of

any analytic expression for the optimal flux tensor ϕ_{ij} associated with åeq:NS1, but the algorithm discussed above can be easily implemented numerically, and our interest will be to explore how the instantaneous optimum fluxes for åeq:NS1 differ from their classical analytic expressions. We will be particularly interested in the tangential flux ϕ_{12}, which is the only one that survives under long-time averaging. Introducing $\langle\rangle$ to denote averaging over wall-parallel planes and time, it follows from åeq:NS1 that

$$\partial_2\langle\phi_{12}\rangle + \langle g_1\rangle = 0. \tag{3.3}$$

Note that the pressure gradient g_1 has been taken outside the divergence in åeq:NS1, because of its obvious physical interpretation as a momentum source. This also allows us to define quantities that are periodic in x_1, including the residual pressure p and the diagonal momentum fluxes ϕ_{jj} (no summation).

We use simulations in a doubly periodic channel with reasonably large streamwise and spanwise dimensions $L_1 \times L_3 = 8\pi h \times 3\pi h$, and $h^+ = 934$ (del Álamo *et al.* 2004). The different variables can then be expanded in Fourier series as in

$$u_i = \widehat{u}_{i,\alpha}(x_2)\exp[\mathrm{i}(\alpha_1 x_1 + \alpha_3 x_3)], \tag{3.4}$$

where $\alpha_k(j) = 2\pi j/L_k$, $j = -\infty\ldots-1,0,1\ldots\infty$, for $k = 1$ or $k = 3$. For the rest of the paper, the dependence of the Fourier coefficients on the wavenumber will be omitted. Consider, for example, the streamwise component of the flux potential equation åeq:poisvec,

$$\partial_{22}\widehat{\lambda}_1 - (\alpha_1^2+\alpha_3^2)\widehat{\lambda}_1 = 2\widehat{S}_1 - \mathrm{i}\alpha_1\widehat{\Pi}, \tag{3.5}$$

$$\widehat{\lambda}_1(0) = \widehat{\lambda}_1(2h) = 0, \tag{3.6}$$

where $\widehat{S}_i$ is the right-hand side of åeq:NS1, and

$$\widehat{\Pi} = \widehat{\nabla\cdot\boldsymbol{\lambda}} = \mathrm{i}\alpha_1\widehat{\lambda}_1 + \partial_2\widehat{\lambda}_2 + \mathrm{i}\alpha_3\widehat{\lambda}_3, \tag{3.7}$$

The fluxes become,

$$\widehat{\phi}_{11} = \mathrm{i}\alpha_1\widehat{\lambda}_1, \tag{3.8}$$

$$\widehat{\phi}_{12} = \widehat{\phi}_{21} = (\partial_2\widehat{\lambda}_1 + \mathrm{i}\alpha_1\widehat{\lambda}_2)/2, \tag{3.9}$$

$$\widehat{\phi}_{13} = \widehat{\phi}_{31} = \mathrm{i}(\alpha_3\widehat{\lambda}_1 + \alpha_1\widehat{\lambda}_3)/2. \tag{3.10}$$

The divergence $\widehat{\Pi}$ satisfies Poisson's equation åeq:poisdiv with unknown boundary conditions. These are handled indirectly, as in the channel simulations of Kim *et al.* (1987). The equation for each Fourier component of the divergence is solved three times: one with its full right-hand side and homogeneous boundary conditions,

$$\partial_{22}\widehat{\Pi}_0 - (\alpha_1^2+\alpha_3^2)\widehat{\Pi}_0 = \widehat{\nabla\cdot\boldsymbol{S}}, \qquad \widehat{\Pi}_0(0) = \widehat{\Pi}_0(2h) = 0, \tag{3.11}$$

and two with a homogeneous right-hand side and unit boundary condition at one wall and zero at the other. For the solution associated with the lower wall,

$$\partial_{22}\widehat{\Pi}_L - (\alpha_1^2+\alpha_3^2)\widehat{\Pi}_L = 0, \qquad \widehat{\Pi}_L(0) = 1, \quad \widehat{\Pi}_L(2h) = 0, \tag{3.12}$$

with an equivalent expression for the upper one, $\widehat{\Pi}_U$. The divergence can then be written as $\widehat{\Pi} = \widehat{\Pi}_0 + a_L\widehat{\Pi}_L + a_U\widehat{\Pi}_U$, which satisfies,

$$\widehat{\Pi}(0) = a_L, \qquad \widehat{\Pi}(2h) = a_U. \tag{3.13}$$

The Poisson problem åeq:poisF1–åeq:poisF2 is solved three times for each λ_i. For example, once for $\widehat{\lambda}_{10}$, with right-hand side $\widehat{S}_1 - \mathrm{i}\alpha_1\widehat{\Pi}_0$, and once for each of $\widehat{\lambda}_{1L}$ and $\widehat{\lambda}_{1U}$, with

right-hand sides $-\mathrm{i}\alpha_1\widehat{\Pi}_L$ and $-\mathrm{i}\alpha_1\widehat{\Pi}_U$, respectively. Again, the solution can be expressed as $\widehat{\lambda}_1 = \widehat{\lambda}_{10} + a_L\widehat{\lambda}_{1L} + a_U\widehat{\lambda}_{1U}$. The process is repeated for $\widehat{\lambda}_2$ and $\widehat{\lambda}_3$, allowing us to compute the divergence of the resulting $\boldsymbol{\lambda}$ from its definition åeq:divfou. The values of this divergence at the two walls are also linear combinations of three terms, two of which are proportional to a_U and a_L. Substituting them in åeq:divBC allows these coefficients to be computed, and the problem to be closed.

3.1. *Fluctuation velocities*

The different components of the fluxes R_{ij} in åeq:NS1bis have very dissimilar magnitudes. Equation åeq:phi12 can be integrated to give $\langle\phi_{12}^+\rangle = \langle\phi_{12}\rangle/u_\tau^2 = 1 - x_2/h$, where $u_\tau^2 = -\langle g_1\rangle$. This is satisfied by all flux definitions, and implies that the mean of ϕ_{12} is $O(1)$ in wall units. However, the classical fluxes given by åeq:NS1bis are found to have standard deviations of order $R_{rms}^+ = O(20-60)$, which can be used as proxies for their integrated euclidean norm. The optimisation procedure reduces these intensities considerably (not shown), but only to $\phi_{rms}^+ = O(10)$. This is important because, if instantaneous fluxes are to be used to study their contribution to the mean momentum transport or to model them in LES, it is useful if their characteristic magnitude is not much larger than their average.

Some reflection shows that the problem is that åeq:NS1–åeq:NS1bis are written in the frame of reference linked to the wall, and that the fluctuating fluxes are dominated by sweeping terms of the type Uu_i', where we have made the customary decomposition, $u_i = U(x_2)\delta_{i1} + u_i'$ with respect to the mean profile $U(x_2) = \langle u_1\rangle$. In terms of the perturbation velocities, the momentum equation becomes,

$$\partial_j\phi_{ij}' = -\partial_t u_i' + g_i - U\partial_1 u_i' + (\nu\partial_{22}U - u_2'\partial_2 U)\delta_{i1}, \tag{3.14}$$

one of whose solutions is

$$\phi_{ij}' = R_{ij}' \equiv u_i'u_j' + p\delta_{ij} - 2\nu\sigma_{ij}', \tag{3.15}$$

with σ_{ij}' defined as in åeq:NS1 using $\boldsymbol{u}'$. When compared with åeq:NS1, most of the extra terms in the right-hand side of åeq:NS2 average to zero over long times, but they can be large instantaneously, and are responsible for the large standard deviations of the fluxes in åeq:NS1bis. For example, it is known experimentally that the standard deviation of the perturbation tangential stress in the logarithmic layer is $(u_1'u_2')_{rms}^+ \approx 2$ (Lozano-Durán *et al.* 2012), but the standard deviation of $(u_1u_2)^+$ is $O(20)$. There is no difference between perturbation and total velocities for the transverse velocity components.

The fluctuation intensities of the perturbation fluxes in åeq:NS2bis are represented in figure 1 as lines with symbols. They are weaker than the values cited above for the fluxes based on the full velocities, and only the standard deviation of $R_{11}'^+$ reaches $O(10)$ near the wall. However, it should be born in mind that these fluxes no longer represent the full momentum transfer, and that part of the momentum is now carried by the linear advection terms in the right-hand side of åeq:NS2. The left-most one, $U\partial_1 u_1'$, is the advection of the velocity fluctuations by the mean velocity profile, and appears as flux fluctuations in any but the semilagrangian frame of reference that follows the mean flow. It was shown in Jiménez (2013*a*) that about 90% of the particle acceleration in a channel flow is due to this term, and this is the main reason why the standard deviation of the fluxes is reduced when defined in terms of fluctuations. The price of this nonuniform frame of reference is the last term in the right-hand side of åeq:NS2, $u_2'\partial_2 U$, which is the classical lift-up representing the change in mean velocity of a fluid particle as it moves with respect to the wall. Whether these transfers should be treated as fluxes or sources has to be decided on physical grounds.

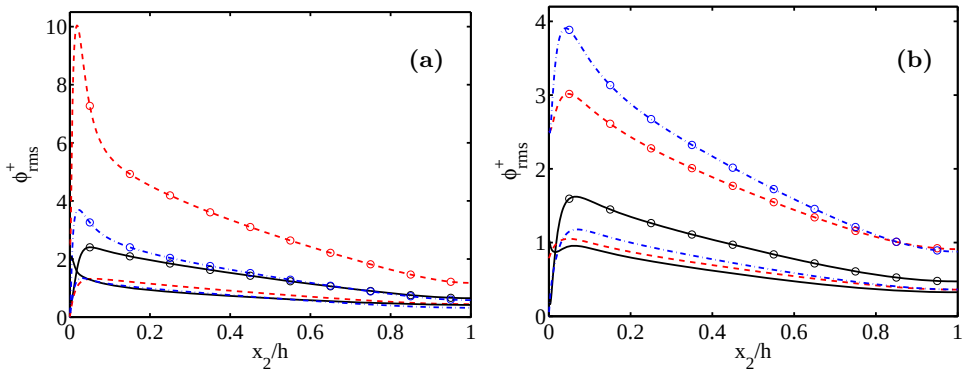

FIGURE 1. Root-mean-squared fluctuation intensities of the momentum fluxes along the three coordinate directions, computed with the fluctuation velocity equation åeq:NS2. (a) Fluxes of the streamwise momentum. − − −, ϕ_{11}; ———, ϕ_{12}; −·−·−, ϕ_{13}. (b) Fluxes of the transverse momenta. − − −, ϕ_{22}; ———, ϕ_{23}; −·−·−, ϕ_{33}. Lines with circles are R'_{ij} from åeq:NS2. Those without symbols are optimum fluxes ϕ'_{ij} from (3.5–3.10).

4. Results

The results of applying the optimisation process to åeq:NS2 are shown in figure 1, where they are compared with the classical algebraic perturbation fluxes R'_{ij}. The optimisation reduces the fluctuating intensity of all the fluxes by a substantial factor that varies among components. In fact, the reduction is larger than shown in the figure, because the standard deviation is computed with respect to the mean value, which is typically not zero for the classical fluxes. For example, $\langle R'_{11}\rangle = \langle {u'_1}^2\rangle \geq 0$, while it follows from åeq:varphisym that the mean value of the optimal diagonal fluxes along any homogeneous direction vanishes identically. All the optimal flux fluctuations are of similar magnitude, and of the order of the mean momentum transfer rate u_τ^2. Note that the standard deviations discussed here refer to the fluctuations of the quadratic functions of the velocities, as in $(u^2)^2_{rms} = \langle u^4\rangle - \langle u^2\rangle^2$, not to those of the velocities themselves.

Although not shown in the figure, the effect of the pressure on the diagonal stresses R'_{ii} in åeq:NS2bis (no summation implied) is not negligible, and always increases the fluctuation intensities when compared with the classical Reynolds products ${u'_i}^2$. This is particularly evident for the wall-normal velocity u_2^2. On the other hand, the effect of the viscous term in R'_{ij} is negligible above $x_2^+ \approx 20$.

The optimal fluxes are also less intermittent than the classical algebraic ones or than the Reynolds products $\tau_{ij} = u'_i u'_j$. Their third-order skewness and fourth-order flatness are given in figure 2(a,b). It is well-known that the Reynolds products are skewed and intermittent, which is clear from the figure, but this is mostly a consequence of their definition as quadratic forms. For example, even if a variable is gaussianly distributed, its square is not, and Antonia & Atkinson (1973) and Lu & Willmarth (1973) showed that the probability distributions of the product $u'_1 u'_2$ is essentially the same as the product of two gaussian variables with the correct cross-correlation coefficient. The theoretical moments for this product of gaussian variables are given in figure 2(a,b), and represent well the observations for the tangential Reynolds product, except very near and far from the wall. The optimal fluxes, which do not suffer from these algebraic artefacts, are much less intermittent and stay approximately gaussian except in the buffer layer. Although not shown in the figure to avoid clutter, the effect of the pressure on R'_{ij} is to decrease intermittency. Particularly for u'^2_2 and u'^2_3, the flatness of the Reynolds products is about

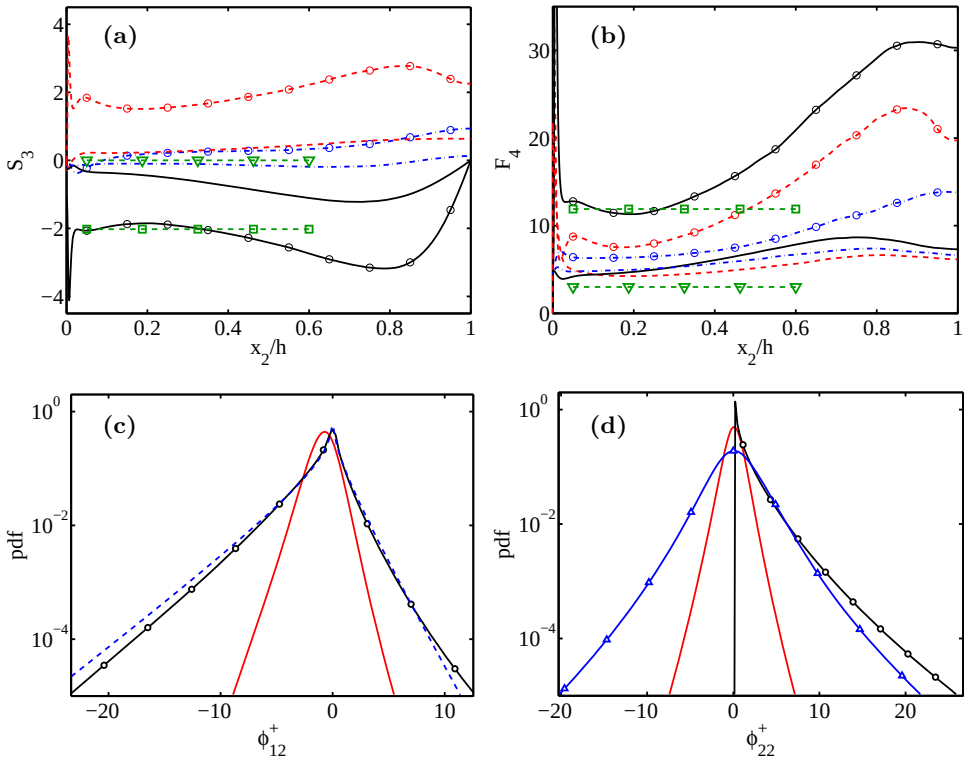

FIGURE 2. Higher-order moments of the fluctuation intensities of the centred momentum fluxes, computed from the fluctuation velocities. – – –, ϕ'_{11}; ———, ϕ'_{12}; –·–·–, ϕ'_{22}. (a) Third-order skewness, $\langle\phi'^3\rangle/\langle\phi'^2\rangle^{3/2}$. (b) Fourth-order flatness. $\langle\phi'^4\rangle/\langle\phi'^2\rangle^2$. The horizontal dashed lines are theoretical values for different functions of gaussian-distributed variables. ▽, A gaussian variable ($S_3 = 0$, $F_4 = 3$); □, the product of two gaussian variables with cross-correlation coefficient -0.4 ($S_3 = -2.02$, $F_4 = 11.9$). (c) Pdf of ϕ_{12} at $x_2/h \in (0.1 - 0.2)$, normalised in wall units. The dashed line is the product of two gaussian variables with cross-correlation coefficient -0.4. (d) As in (c), for ϕ_{22}. The line with triangles is for $u_2'^2 + p$. In all figures, lines with circles are the Reynolds products, $u'_i u'_j$, and those without symbols are optimum fluxes from (3.5–3.10).

three times higher than for the corresponding R'_{ii}, but the effect of the viscous term is also negligible in this case.

The probability density functions (pdfs) for two flux components in the 'logarithmic' layer are given in figure 2(c,d), where both the smaller standard deviation and the weaker intermittency are clear. In the case of τ_{12} in figure 2(c), the figure also shows the theoretical pdf for the product of two gaussian variables, which fits the classical Reynolds product well except at the extreme tails. Note that the mean value of these two pdfs should be exactly the same, $\langle\phi^+_{12}\rangle = x_2/h - 1$, but is achieved by the two fluxes in different ways, While the pdf of the classical Reynolds product peaks at $\tau_{12} = 0$, and owes its negative mean value to the skewness of its tails, the distribution of the optimal fluxes is roughly symmetric about its negative mean value.

Figure 2(d) displays the pdf of the diagonal stress ϕ_{22}. It also shows the narrower distribution of the optimal flux and its narrower tails, although the main difference in this case is that the classical product, $u_2'^2$, is intrinsically positive. The figure also shows the effect of the pressure, discussed at the beginning of this section. Its main effect is to restore the approximate symmetry of the pdf of $u_2'^2 + p$, which now includes negative values. As mentioned above, this also decreases intermittency, although figure 2(d) shows

(a)

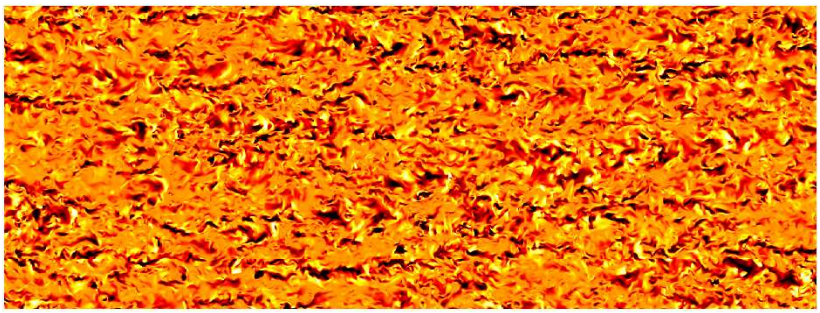

(b)

FIGURE 3. Wall-parallel snapshots of the instantaneous tangential momentum flux in a channel at $Re_\tau = 934$ (del Álamo *et al.* 2004) and $x_2/h = 0.15$. Flow is from left to right, and the area in the figures is $L_1 \times L_3 = 4\pi h \times 3\pi h/2$. (a) Classical flux R'_{12} from åeq:NS2bis. (b) Optimal flux ϕ'_{12}. In both cases, the flux is centred with its mean value, and the colour scale spans ± 3 standard deviations, increasing from dark to light.

that most of this decrease is due to the effect of centring the one-sided pdf of the square. One the other hand, there almost no difference between the pdf of the optimum ϕ'_{22} and that of its traceless equivalent, $\phi'_{22} - \Pi'/3$ (not shown).

Reynolds and optimal fluxes are also structurally quite different. This is shown in figures 3(a,b), where the classical transverse Reynolds stress $R'_{12} \approx u'_1 u'_2$, is compared with the corresponding optimal flux ϕ'_{12}. Both quantities are shown centred with respect to their mean and normalised with their standard deviation. This scaling absorbs the difference in their magnitude, but the geometry of the field remains different. This is partly because of the stronger intermittency of R'_{12}, manifested by the presence of numerous dark and light spots in figure 3(a), but the characteristic streamwise organisation of the Reynolds stresses is much less marked in the optimal flux in figure 3(b).

This is confirmed by the spectra in figure 4, where ϕ'_{12} is compared to R'_{12}. Note that these spectra are different from the cospectrum of u'_1 and u'_2, which is included in figure 4(a) for comparison. The latter represents the contribution of the product τ_{12} to the mean tangential stress, while the former reflect the geometry of the product (Lozano-Durán *et al.* 2012). Figure 3(a) shows two-dimensional spectra in the plane $x_2/h = 0.15$, and reveals that the cospectrum is dominated by the elongated streaks of the streamwise velocity. In the case of products of velocities, the high-order spectra were shown by Van Atta & Wyngaard (1975) to be dominated by the sweeping of the small scales by the larger ones, and the spectrum of R'_{12} is also anisotropic, although less than the cospectrum. On the other hand, the spectrum of ϕ'_{12}, which is only indirectly linked to u_1 through

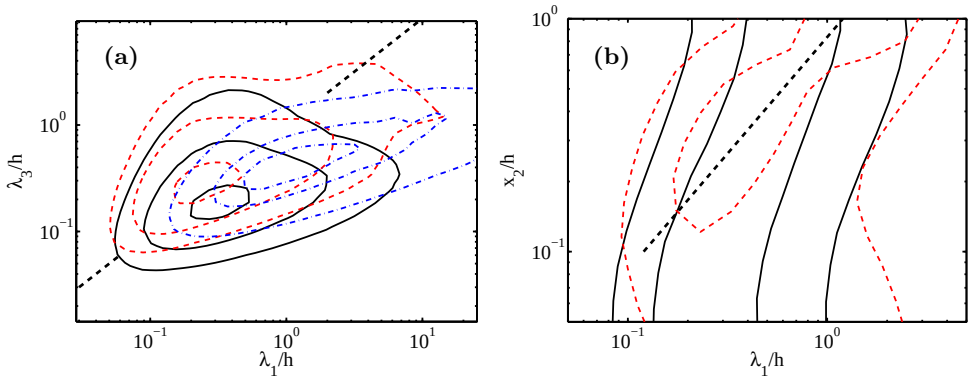

FIGURE 4. (a) Two-dimensional premultiplied spectra as functions of the wall-parallel wavelengths. ———, R'_{12}; − − −, optimal ϕ'_{12}; −·−·−, cospectrum of u'_1 and u'_2. The three contours contain 10%, 50% and 80% of the spectral mass. The dashed diagonals are $\lambda_1 = \lambda_3$. Flow as in figure 3, $x_2/h = 0.15$. (b) Streamwise premultiplied spectra, as a function of x_2. Each horizontal section is a spectrum normalised to unit energy, and the contours are 50% and 80% of the global maximum. ———, R'_{12}; − − −, ϕ'_{12}. The dashed diagonal is $\lambda_1 = 1.2\,x_2$.

the right-hand side of êq:NS2, is only weakly influenced by the elongated streaks, and is more isotropic (i.e., closer to $\lambda_1 = \lambda_3$).

Figure 4(b) shows one-dimensional pre-multiplied spectra as functions of the streamwise wavelength and of the distance to the wall. It is known that the wavelength of the maximum of the cospectrum increases linearly with x_2 at high Reynolds numbers (see figure 1b in Jiménez 2012), but this is still not obvious at the relatively low Reynolds number of figure 4. The reason is that R'_{12} is dominated by the effect of the wall-parallel velocity u'_1, whose scale is not constrained by the impermeability condition near the wall (Townsend 1961). On the other hand, figure 4(b) shows that the ϕ'_{12}, which is free from spurious influence of the inactive wall-parallel motion, grows linearly away from the wall even at this relatively low Reynolds number. It can be shown that the difference between the spectrum of classical and optimal fluxes is largest in the buffer layer, and decreases with increasing distance to the wall. This effect is more marked for quantities involving u'_1 or u'_3, and almost nonexistent for ϕ_{22}.

Note that the gauge freedom in the definition of the momentum fluxes calls into question the meaning of individual structures of intense Reynolds products, such as those studied in the classical 'quadrant' classification of the (u'_1, u'_2) plane by Wallace *et al.* (1972) and Lu & Willmarth (1973), and in modern three-dimensional extensions of the same idea by Lozano-Durán *et al.* (2012); Lozano-Durán & Jiménez (2014). Although a detailed investigation of this question is beyond the scope of this paper, the present results suggest that these structural analyses should be repeated using other gauges, such as the present optimal one, to test how dependent on the gauge are the properties of the resulting structures. This is a case in which intermittency is beneficial, since the hope is to identify structures strong enough to stay coherent independently of the rest of the flow, but able to explain some flow characteristics from a small fraction of the total volume. The weaker intermittency of the optimal fluxes in figure 2 suggests that analyses based on intense structures may be less relevant for them than for the classical Reynolds products. For example, it follows from the pdfs in figure 2(c) that, while the 10% strongest points of $-\tau_{12}$ contain around 70% of the total Reynolds stress, the equivalent strongest 10% of the optimal $-\phi'_{12}$ only accounts for 33%. Correspondingly,

the volume fraction of the 'countergradient' momentum flux, defined as $\phi_{12}\partial_2 U > 0$, is approximately 15% for the optimal fluxes in the logarithmic layer, and 30% for τ_{12}.

5. Discussion and conclusions

We have seen that the fluxes implicit in conservation laws are not uniquely defined, in a way similar to the gauge ambiguity of classical field theory. As an example, we have developed a particular definition that minimises the integral of their square. Although this definition should not be considered in any way unique, it has the intuitive appeal of generating minimum 'sterile circularity' in the transfers of the conserved quantity. We have presented a way to compute such fluxes from simulations, and applied it to the momentum transfer in turbulent channels. Of particular interest is that the results differ substantially from the classical Reynolds stresses, whose main justification appears, in this light, to be that they have become easier to interpret through familiarity, and that they are obtained from a particularly convenient algebraic manipulation of the equations of motion.

The present results raise some interesting questions that go beyond the scope of the present paper, and which should eventually be considered individually. Not the least of them is whether, given their arbitrariness, point-wise Reynolds stresses should be considered to be proper targets for the sub-grid models of large-eddy simulations (LES) or, up to point, of Reynolds-averaged models. Only their divergence is important, while the stresses themselves can vary widely without ill effects. This may help explain the apparent contradiction that 'a-priori' testing of many LES models fails grossly while the 'a-posteriori' results are reasonable (Bardina 1983). It is interesting to note in this context that the very successful dynamic model (Germano *et al.* 1991) can be characterised as an algorithm to determine the magnitude of the eddy viscosity from the difference of the subgrid stresses at two different scales, and can therefore be seen as an integral implementation of fitting the divergence of the fluxes in scale space, rather than the fluxes themselves.

Also interesting is that åq:divn–åq:divnR provides an algorithmic 'accounting' definition of fluxes that can be computed even in cases in which the physical formulation is difficult to interpret locally. There is no implication that the result can be expressed in terms of a 'formula' of local variables, but this is no worse than for the pressure, which is part of the classical momentum and energy fluxes, and can only be determined as the solution of a partial differential equation. Numerically, all variables are equally simple to obtain, particularly since åq:divnR ensures that any expression for the fluxes provides a way to compute all other representations.

For example, the Kolmogorov inertial energy cascade assumes that energy is transferred across scales from its injection into large structures to its dissipation in small viscous ones. Defining the energy flux, ε, is straightforward in isotropic flows for which scale is a one-dimensional parameter, and the conservation equation åq:divn can be solved by a simple quadrature. In more general cases the definition is not so clear, and any attempt to write energy conservation in spectral space leads to a formulation in terms of wavenumber triads that cannot be interpreted locally. This ambiguity is at the root of many of the discussions about the instantaneous direction of energy transfer and of the relevance of backscatter. An energy equation equivalent to åq:divn in wavenumber space provides a definition of a vector energy-transfer rate that is local, algorithmically computable and, inasmuch as energy conservation embodies the behaviour of the energy, as physically 'relevant' as any definition based on algebraic expressions. Note that even the classical one-dimensional definition of ε relies on a homogeneous boundary condition

such as åeq:varbc. The energy transfer rate can only be given a definite value by assuming that it vanishes at very large and very small scales.

An even more interesting application concerns non-homogeneous flows. While the concept of scale is unambiguous in homogeneous flows, it is harder to define in inhomogeneous ones, where it is not easily separated from position. One of the central results of harmonic analysis is that position and scale cannot be exactly defined at the same time. Consider, for example, a turbulent channel in which energy is being transferred among eddies of different sizes while they move relative to the wall. The ambiguity is whether their energy should be considered as being transferred across space or across scale. A recent analysis of this problem led to an equation for the transfer of the second-order structure function (the 'scale energy') in the form of a double divergence, in space and scale, of a six-dimensional vector flux (Hill 2002),

$$\partial_{x_j}\phi_j + \partial_{r_j}\psi_j = S, \tag{5.1}$$

where x_j with $j = 1\ldots3$ represent the spatial directions, and r_j are the respective separations along those directions. The analysis provides explicit expressions for the fluxes in space, ϕ_j, and scale, ψ_j, which have been computed and interpreted in turbulent channels by Cimarelli & De Angelis (2011) and Cimarelli & De Angelis (2012). They are not optimal in the sense described above (Cimarelli, private communication). Irrespective of the merits of the structure function as a measure of energy at a given scale, the previous considerations show that these fluxes and this analysis are not unique, and suggest that their conclusions should be revisited in terms of their robustness with regards to the different definitions.

In general, cascade theories concern themselves with fluxes, which are typically conserved across some 'inertial' range. The quantities being transferred, such as the energy, are typically created and dissipated somewhere else in the system. The results in the present paper suggest that the concept of flux, and therefore of cascades, should be re-examined with care.

This work was supported by the European Research Council Coturb grant ERC-2014.AdG-669505. I am grateful to the Sidney Sussex College and to the department of Engineering of the U. of Cambridge for their hospitality during the preparation of this manuscript.

REFERENCES

del Álamo, J. C., Jiménez, J., Zandonade, P. & Moser, R. D. 2004 Scaling of the energy spectra of turbulent channels. *J. Fluid Mech.* **500**, 135–144.

Antonia, R. A. & Atkinson, J. D. 1973 High-order moments of Reynolds shear stress fluctuations in a turbulent boundary layer. *J. Fluid Mech.* **58**, 581–593.

Van Atta, C. W. & Wyngaard, J. C. 1975 On higher-order spectra of turbulence. *J. Fluid Mech.* **72**, 673–694.

Bardina, J. 1983 Improved turbulence models based on large eddy simulation of homogeneous, incompressible, turbulence flows. PhD thesis, Thermosciences Div., Dept. of Mech. Engng., Stanford Univ.

Barut, A. O. 1980 *Electrodynamics and classical theory of fields and particles*. Dover.

Cimarelli, A. & De Angelis, E. 2011 Analysis of the Kolmogorov equation for filtered wall-turbulent flows. *J. Fluid Mech.* **676**, 376–395.

Cimarelli, A. & De Angelis, E. 2012 Anisotropic dynamics and sub-grid energy transfer in wall-turbulence. *Phys. Fluids* **24**, 015102.

Gelfand, I. M. & Fomin, S. V. 1963 *Calculus of variations*. Prentice-Hall.

Germano, M., Piomelli, U., Moin, P. & Cabot, W. 1991 A dynamic subgrid-scale eddy viscosity model. *Phys. Fluids A* **3**, 1760–1765.

Hill, R. J. 2002 Exact second-order structure-function relationships. *J. Fluid Mech.* **468**, 317–326.

Jiménez, J. 2012 Cascades in wall-bounded turbulence. *Ann. Rev. Fluid Mech.* **44**, 27–45.

Jiménez, J. 2013*a* How linear is wall-bounded turbulence? *Phys. Fluids* **25**, 110814.

Jiménez, J. 2013*b* Near-wall turbulence. *Phys. Fluids* **25**, 101302.

Kim, J., Moin, P. & Moser, R. D. 1987 Turbulence statistics in fully developed channel flow at low Reynolds number. *J. Fluid Mech.* **177**, 133–166.

Kolmogorov, A. N. 1941 The local structure of turbulence in incompressible viscous fluids a very large Reynolds numbers. *Dokl. Akad. Nauk. SSSR* **30**, 301–305, reprinted in *Proc. R. Soc. London.* A **434**, 9–13 (1991).

Lozano-Durán, A., Flores, O. & Jiménez, J. 2012 The three-dimensional structure of momentum transfer in turbulent channels. *J. Fluid Mech.* **694**, 100–130.

Lozano-Durán, A. & Jiménez, J. 2014 Time-resolved evolution of coherent structures in turbulent channels: characterization of eddies and cascades. *J. Fluid Mech.* **759**, 432–471.

Lu, S. S. & Willmarth, W. W. 1973 Measurements of the structure of the Reynolds stress in a turbulent boundary layer. *J Fluid Mech* **60**, 481–511.

Townsend, A. A. 1961 Equilibrium layers and wall turbulence. *J. Fluid Mech.* **11**, 97–120.

Townsend, A. A. 1976 *The structure of turbulent shear flow*, 2nd edn. Cambridge U. Press.

Wallace, J. M., Eckelmann, H. & Brodkey, R. S. 1972 The wall region in turbulent shear flow. *J. Fluid Mech.* **64**, 39–48.